

# Germanium-based quantum emitters towards *time-reordering entanglement scheme* with degenerate exciton and biexciton states

Nicola Dotti,<sup>1</sup> Francesco Sarti,<sup>1</sup> Sergio Bietti,<sup>2</sup> Alexander Azarov,<sup>3</sup> Andrej Kuznetsov,<sup>3</sup> Francesco Biccari,<sup>1</sup> Anna Vinattieri,<sup>1</sup> Stefano Sanguinetti,<sup>2</sup> Marco Abbarchi,<sup>4,\*</sup> and Massimo Gurioli<sup>1,†</sup>

<sup>1</sup>*LENS, Dipartimento di Fisica, Università di Firenze, Via Sansone 1, I-50019 Sesto Fiorentino, Italy*

<sup>2</sup>*L-NESS and Dipartimento di Scienza dei Materiali, Università di Milano Bicocca, Via Cozzi 53, I-20125 Milano, Italy*

<sup>3</sup>*Department of Physics, University of Oslo NO-0316 Oslo (Norway)*

<sup>4</sup>*CNRS, Aix-Marseille Université, Centrale Marseille, IM2NP, UMR 7334, Campus de St. Jérôme, 13397 Marseille, France*

(Dated: October 26, 2021)

We address the radiative emission of individual germanium extrinsic centers in  $\text{Al}_{0.3}\text{Ga}_{0.7}\text{As}$  epilayers grown on germanium substrates. Micro-photoluminescence experiments demonstrate the capability of high temperature emission (70 K) and complex exciton configurations (neutral exciton X and biexciton XX, positive  $X^+$  and negative  $X^-$  charged exciton) of these quantum emitters. Finally, we investigate the renormalization of each energy level showing a large and systematic change of the binding energy of XX and  $X^+$  from positive to negative values (from  $\sim +5$  meV up to  $\sim -7$  meV covering about  $\sim 70$  meV of the emission energy) with increasing quantum confinement. These light emitters, grown on a silicon substrate, may exhibit energy-degenerate X and XX energy levels. Furthermore, they emit at the highest detection efficiency window of Si-based single photon detectors. These features render them a promising device platform for the generation of entangled photons in the *time-reordering scheme*.

## I. INTRODUCTION

The implementation of quantum states of light is at the base of most quantum computation and quantum information protocols:<sup>1-3</sup> bright and high-quality single-, entangled- and indistinguishable-photon emitters are a necessary resource for quantum key distribution, quantum repeaters and photonic quantum information processing.<sup>4-7</sup> In the same field, other important applications of solid-state quantum-sources consist in the possibility to couple them with atomic vapours for the production of quantum-bit based on slow-light memories<sup>8,9</sup> or on electron and holes spin.<sup>10-12</sup> Single photon emission<sup>13,14</sup> has been demonstrated in several solid state systems such as epitaxial and colloidal quantum dots,<sup>15-29</sup> carbon nanotubes<sup>30</sup> and single molecules.<sup>31-33</sup>

More advanced implementations of quantum states of light, such as entangled photon pairs, can be obtained in solid state systems, provided the binding of two correlated electronic states within the same nanostructure.<sup>4,15,20,26-28,34</sup> Several schemes for the generation of entangled photons have been proposed for quantum dots. Most of them are based on the neutral biexciton-exciton cascade XX-X: provided the implementation of a spin-degenerate neutral exciton transition, a maximally entangled photon pair can be encoded in the polarization degree of XX and X photons. The requirement of spin degeneracy can be satisfied for negligible electron-hole spin interaction allowing to erase the *which-path information* in the biexciton-exciton cascade. This kind of spin-degenerate state has been implemented either as an *a priori*, built-in characteristic of the nanostructure (like in Reference 26 where highly symmetric and unstrained quantum dots were grown<sup>35-37</sup>), by spectral filtering the photons having the same energy<sup>38</sup> or by tuning *a posteriori* the fine interaction to zero.<sup>20,25,28,34</sup>

A different protocol called *time-reordering scheme*, has been recently proposed in order to implement polarization en-

tanglement in the emitted photon cascade (XX-X) from QDs with arbitrary spin-splitting.<sup>39,40</sup> This scheme is based on the zero biexciton binding energy allowing to erase the *which-path information* by introducing *a posteriori* and *ad-hoc* delay of the XX-X emitted photons. The time-reordering protocol relaxes the need of a perfectly spin-degenerate neutral exciton state, but the condition of zero biexciton binding energy is not straightforward to be realized, and this photon entanglement scheme has not been yet experimentally demonstrated. Still there are a few reports on QDs naturally exhibiting degenerate XX and X states<sup>41-44</sup> or on the possibility of tuning *a posteriori* the XX binding energy to zero with an external control.<sup>25,28,34</sup>

A second relevant route to obtain quantum light sources in semiconductor devices in alternative to conventional QDs, is related to the exploitation of extrinsic centers in III-V, IV and II-VI semiconductor alloys.<sup>45-48</sup> Single photon emission from isolated impurity centers has been shown in ZnSe/ZnMgSe alloys,<sup>49</sup> tellurium isoelectronic dyads in ZnSe,<sup>50</sup> nitrogen impurity centers in GaAs<sup>51-54</sup> and in AlAs<sup>55</sup> and with nitrogen-vacancy centers and chromium in diamonds.<sup>52,56-61</sup>

Within this class of quantum emitters, some impurity centers (for example dyads complexes<sup>50,55</sup>) allow to confine exciton complexes, thus leading to the possibility to be exploited as sources of entangled photons. Nevertheless, for extrinsic centers, the scientific literature on XX-X cascade is much less flourished with respect to QDs and, for example, the possibility to obtain time-reordering has not yet been reported. Among several interesting features, a peculiar properties of extrinsic centers is the possibility to exploit them in indirect band-gap based devices, such as carbon<sup>62,63</sup> and copper<sup>64,65</sup> impurity centers in silicon and carbon antisite-vacancy pairs in SiC.<sup>66</sup> This last example has been demonstrated to be a bright single photon emitter at room temperature.

In a recent paper, we showed a hybrid III-V/IV-IV single photon device based on extrinsic emitters in  $\text{Al}_{0.3}\text{Ga}_{0.7}\text{As}$ <sup>67</sup>

fabricated with a low thermal budget method on Ge and Si substrates, thus providing a solid-state platform towards the integration of quantum light sources in *classical* electronic devices.

In this paper we firstly unambiguously demonstrate, by a comparative analysis with samples grown in different conditions, the connection of these latter extrinsic emitters<sup>67</sup> with Ge contamination of the  $\text{Al}_{0.3}\text{Ga}_{0.7}\text{As}$  alloy. Then, by a careful micro-photoluminescence analysis we are able to imaging a large sample region isolating a large ensemble of extrinsic defect and determining their density and *pseudo-macro-photoluminescence* spectrum. We also perform a statistical analysis of the excitonic complexes from these Ge-centers, demonstrating the change from binding to anti-binding of the biexciton  $\text{XX}$  and positive charged exciton  $\text{X}^+$  states with the increase of the emission energy of the corresponding neutral exciton transition  $\text{X}$ , thus opening the possibility to implement a *time reordering scheme* for  $\text{XX-X}$  photon cascade exploiting defects in semiconductors. We finally validate their photostability at high temperature and show a selective quantum-confined-Stark effect as the main origin of the different inhomogeneous line broadening of the s-shell bright states (the two neutral states  $\text{X}$  and  $\text{XX}$ , plus the positive and negative charged excitons,  $\text{X}^+$  and  $\text{X}^-$  respectively). It is important noting that the devices in use were grown on standard Ge substrates and they emit in the spectral interval of highest detection efficiency of most single-photon silicon-based light-detectors.

The paper is organised as follows: in Section II we provide a description of the experimental setup used for the micro-photoluminescence (micro-PL) investigation and the sample fabrication; In Section III we precisely address the origin of the extrinsic centers as Ge related defects, comparing purely III-V (Ge-free samples) with samples grown on a germanium substrate. In addition we map the Ge-centers emission over large areas thus enabling the precise isolation of the related *pseudo-macroPL* ensemble emission. In Section IV the high-power excitation regime is discussed showing the onset of multiexcitonic and charged exciton features. We also discuss the photostability at high temperature of individual Ge-centers as well as the quantum confined Stark-effect originated from charged defects in the surrounding semiconductor matrix. Finally, in Section V, we discuss the features of the binding energy of  $\text{XX}$ ,  $\text{X}^+$  and  $\text{X}^-$  showing the transition from binding to anti-binding of  $\text{XX}$  and  $\text{X}^+$ . In Section VI we draw the conclusions.

## II. EXPERIMENTAL: SAMPLE PREPARATION AND EXPERIMENTAL METHODS

A thorough description of the device in use can be found in reference 67 and 68 where first evidences of excitonic recombination and single photon emission were shown for Ge-impurities in  $\text{Al}_{0.3}\text{Ga}_{0.7}\text{As}$  grown on germanium and silicon substrates. The results found for the two different kind of substrates are very similar and here we concentrate our attention only on the Ge-substrate case. A scheme of the sample cross

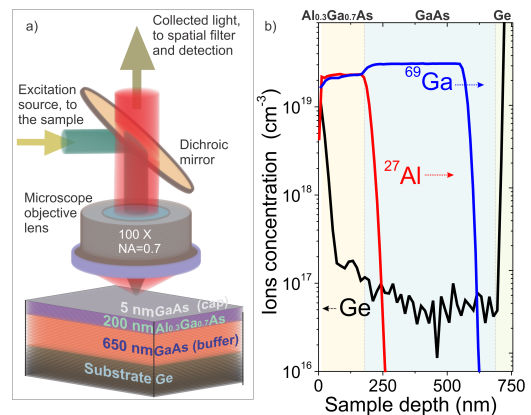


FIG. 1. a) Bottom, sketch of the sample composition: 5 nm GaAs (capping layer), 200 nm  $\text{Al}_{0.3}\text{Ga}_{0.7}\text{As}$  (active layer), 650 nm GaAs (buffer layer), Ge (substrate). Top, scheme of the optical apparatus used for PL experiments. b) SIMS measurements on the investigated sample. Ge (left axis, calibrated), Ga and Al (right axis, not calibrated) ions concentration are plotted in a logarithmic scale as a function of the milled depth. Shaded areas highlight the different layers.

section is given in the bottom part of Fig. 1a) (this sample will be denoted as Ge 580 °C in the following).

As references, we grew two test-samples with similar parameters of those described before but on conventional GaAs substrates and, in one case, also using low temperature growth in order to facilitate possible Al clustering. For the first test sample on GaAs we grew a 200 nm  $\text{Al}_{0.3}\text{Ga}_{0.7}\text{As}$  layer at 580 °C for the first 100 nm, 400 °C for the central 30 nm and again 580 °C for the last 70 nm (this sample will be denoted as GaAs 400 °C in the following). In the second test sample the temperature was set at 580 °C for the full 200 nm  $\text{Al}_{0.3}\text{Ga}_{0.7}\text{As}$  thickness (this sample will be denoted as GaAs 580 °C in the following).

For micro-PL experiments the samples were kept at low temperature in a low-vibration liquid He-flow cold-finger cryostat which in turn was mounted on a stepping motor translation-stage for scanning the sample surface. A schematic view of the experimental setup is shown in the top part of Fig. 1 a). More details are given in reference 67 and 68

In the case of the Ge 580 °C sample, the Ge concentration versus depth profiles was measured by secondary ion mass spectrometry (SIMS) with a Cameca IMS 7f microanalyzer (the Ge detection limit was estimated in  $\sim 5 \times 10^{16} \text{ cm}^{-3}$ ). A 10 keV  $\text{O}^{2+}$  primary beam with a current of 600 nA was rastered over a  $150 \times 150 \mu\text{m}^2$  area and secondary ions were collected from the central part of the sputtered crater. The intensity-concentration calibration was performed using Ge ion implanted samples as a reference. The conversion from sputtering time to sample depth was performed by measurement of the crater depth using a Dektak 8 stylus profilometer and assuming a constant erosion rate.

The results of SIMS measurements are shown in Fig. 1 b) in a logarithmic scale as a function of the milled depth. A

large Ge concentration is found in both the GaAs buffer and  $\text{Al}_{0.3}\text{Ga}_{0.7}\text{As}$  layer, denoting a Ge diffusion from the substrate into the MBE grown layers. Here the Ge contamination reaches the value of  $\rho_{\text{Ge}} \simeq 10^{17} \text{ cm}^{-3}$  (not very different from the values reported in references 69 and 70 for similar samples), sufficiently large to form an impurity band. Indeed, according to the Mott criterion for GaAs, the critical doping  $n_c$  to form a band (defined as  $a_B n_c^{1/3} = 0.25$ , where  $a_B$  is the Bohr radius), is  $n_c \simeq 1.3 \times 10^{16} \text{ cm}^{-3}$ .<sup>53</sup> The relatively large Ge contamination of the  $\text{Al}_{0.3}\text{Ga}_{0.7}\text{As}$  alloy is an important clue for the attribution of extrinsic quantum emitters to Ge-centers, which will be discussed in the following. The large increase of the Ge content near the surface (first 50 nm, see Fig. 1 b)) is likely due to segregation of Ge on the GaAs surface during the growth and/or Ge out-diffusion towards the surface.

### III. NATURE OF THE DEFECTS AND ENSEMBLE SPECTRA

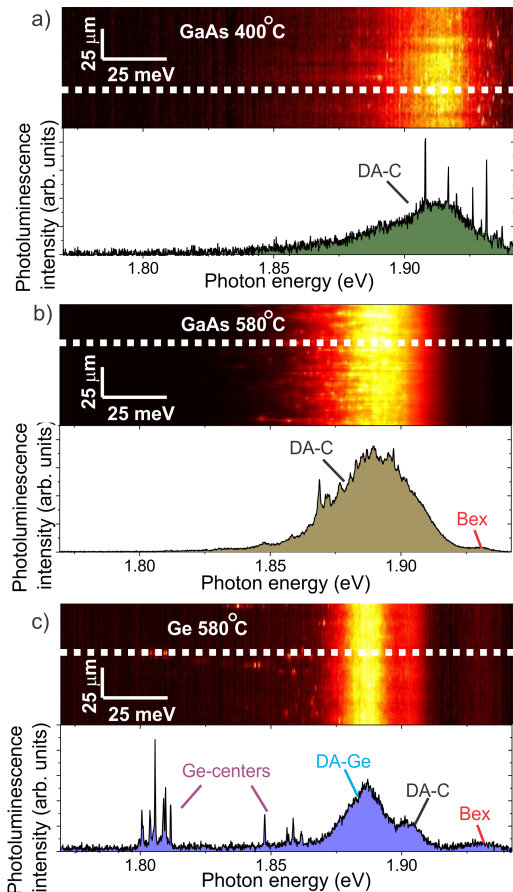


FIG. 2. a), b) and c) Top panel shows a 1D scan over  $100 \mu\text{m}$  (in  $0.5 \mu\text{m}$  steps) on samples GaAs  $400^\circ\text{C}$ , GaAs  $580^\circ\text{C}$  and Ge  $580^\circ\text{C}$ . The white dashed line highlights the spatial position of the spectrum shown in the corresponding bottom panel. Bottom panels: typical PL spectrum extracted from the 1D scan in the top panel.

Before addressing the optical properties of the extrinsic quantum emitters in  $\text{Al}_{0.3}\text{Ga}_{0.7}\text{As}$  we unambiguously validate their origin as due to Ge centers by comparing the emission of purely III-V samples with that of those grown on silicon and germanium. This is also done in order to exclude the presence of Al-poor clusters in the  $\text{Al}_x\text{Ga}_{1-x}\text{As}$  matrix. In fact, the presence of such Al-poor zones has been recently proposed<sup>71,72</sup> as possible explanation of bright and sharp PL lines (emitting from  $\sim 1.7 \text{ eV}$  up to  $\sim 2 \text{ eV}$ ) in  $\text{Al}_x\text{Ga}_{1-x}\text{As}$  nanowires.<sup>67,68</sup> Note that the excitonic emission from those clusters<sup>71,72</sup> falls in a similar spectral interval of the Ge-defects emission investigated here (emitting from  $\sim 1.8 \text{ eV}$  up to  $\sim 1.87 \text{ eV}$ ).

In order to promote some alloy disorder, possibly producing Al-poor nanoclusters within the  $\text{Al}_{0.3}\text{Ga}_{0.7}\text{As}$  layer, we grew the two reference samples GaAs  $400^\circ\text{C}$  and GaAs  $580^\circ\text{C}$ . The micro-PL spectra at low temperature (10 K) of the two test samples are compared with the  $\text{Al}_{0.3}\text{Ga}_{0.7}\text{As}$  layer grown on Ge substrate in Fig. 2. 1D maps (energy vs space), with the detected PL intensity represented as a false-color scale, are shown for each of the three samples. The top panel of Fig. 2 a), b) and c) displays the full scan ( $100 \mu\text{m}$  long) while the bottom panel shows a typical spectrum collected in a single point. In all the three samples we can identify the bound exciton emission (Bex) and the usual band from shallow centers due to carbon-related residual contamination (DA-C).<sup>73,74</sup> This latter band is usually present in AlGaAs layers grown by molecular beam epitaxy.<sup>73-76</sup> By comparing the BEX and DA-C PL bands in the three spectra, we conclude that the Al content is about 5% larger in the GaAs  $400^\circ\text{C}$  sample with respect to the  $580^\circ\text{C}$  sample. At the same time the Al content of the Ge  $580^\circ\text{C}$  sample is slightly larger (of the order of 1%) than the GaAs  $580^\circ\text{C}$  sample. Apart from these unintentional differences in the calibration of the  $\text{Al}_x\text{Ga}_{1-x}\text{As}$  alloy, we note a relevant structuring of the DA-C band with sharp lines spatially localised, together with an overall reduced emission efficiency for the lower growth temperature and a broader extension of the DA-C band when compared with a similar sample grown at  $650^\circ\text{C}$  (not shown).

Quite peculiar is the PL spectrum of the sample grown on a Ge substrate where, besides the presence of the same PL structures (DA-C band and BEX band), we observe two other contributions at lower energy (see Fig. 2 c) and previously reported data in references 67 and 68). These two new PL contributions appear as a broad PL band at about  $\sim 1.88 \text{ eV}$  together with, at lower energies, a tail extending till  $\sim 1.80 \text{ eV}$  where several sharp, isolated and bright lines organised in *multiplets* are found. Due to the relevant Ge contamination determined by the SIMS measurements reported in Fig. 1 b), the broad band at around  $\sim 1.88 \text{ eV}$  is ascribed to Ge-related donor-acceptor recombination (it will be denoted as DA-Ge band in the following).<sup>73-76</sup> Similarly to the case of the DA-C band, also the DA-Ge band may show sharp and spatially localised lines. Finally and accordingly with the previous literature, the tail extending to lower energy is interpreted as emission from deep donor-acceptor levels.<sup>47,77-79</sup>

In two recent papers, we showed that the sharp lines emissions below the DA-Ge band show antibunching and biexciton

recombination.<sup>67,68</sup> The comparison with Ge free samples and the data from SIMS measurements, demonstrate that the Al-poor nanoclusters, leading to natural QDs in the  $\text{Al}_x\text{Ga}_{1-x}\text{As}$  alloy (as observed in Ref 71 and 72), do not play a role in the attribution of the sharp lines organised in localised multiplets which are observed only in the sample grown on the Ge substrate. This new findings lead us to conclude that the extrinsic centers under investigation have to be ascribed to the presence of Ge contamination in the  $\text{Al}_{0.3}\text{Ga}_{0.7}\text{As}$  layer.

We now focus the attention on the case of the sample grown on a germanium substrate by performing extended 2D PL maps at low excitation power. In Fig. 3 a) we highlight three spectral intervals: I for Ge-impurities emission, II for the DA-Ge and DA-C emission and zone III for the BEx emission. In Fig.3 b) are displayed the results of a surface scan spectrally integrated over the three intervals highlighted in Fig.3 a). We observe a strong spatial localization of the emitted intensity from the spectral interval I (Fig.3 b) left panel) in bright spots which lateral extension in space reflects our instrumental resolution. For the zones II and III instead (Fig.3 b) central and right panels respectively), a rather uniform intensity distribution is observed (see also the maps reported in the supplementary materials Supplementary Material 80 and 81). The dark area in the top right part of the images is attributed to an extended defect of the crystal or to some impurity on the sample surface.

The micro-PL mapping allows for a precise counting of the emitting Ge-impurities within the investigated sample surface (and sample thickness). Integrating over two maps of  $50 \times 50 \mu\text{m}^2$  we find a surface density of spatially localised and sharp peaks of about  $\sim 2.5 \times 10^{-2} \mu\text{m}^{-2}$ . By taking into account the thickness of the  $\text{Al}_{0.3}\text{Ga}_{0.7}\text{As}$  layer, we evaluate a concentration of  $\rho_{PL} \simeq 10^{11} \text{cm}^{-3}$  which is by far smaller than the concentration of Ge ions measured in SIMS  $\rho_{Ge} \sim 10^{17} \text{cm}^{-3}$  (see Fig. 1 b)).

The low density of quantum emitters and their PL-spectra with multiple lines is an indication of the complex nature of these extrinsic centers. As for similar systems of extrinsic centers able to accommodate multiexcitonic states,<sup>51-55</sup> we believe that a likely attribution of the defects responsible for the isolated emission below 1.87 eV can be the presence of binary systems or more generally, complex defects. As an example, let us explicitly refer to the attribution of N-dyads in AIAs as responsible of biexciton emission<sup>55</sup> and tentatively assume that our extrinsic centers were related to pairs of Ge impurities. With this hypothesis and assuming a stochastic model<sup>45,55</sup> it is possible to compare the measured density of emitting centers ( $\rho_{PL}$ ) with that of pairs of Ge ions ( $\rho_{Ge-Ge} = \rho_{Ge}^2 V$  where  $V = d_{Ge-Ge}^3$  is the volume occupied by a pair). We can roughly estimate the typical distance between two ions  $d_{Ge-Ge}$  in the  $\sim 0.1 \text{ nm}$  range which well compares with the lattice constant of the host semiconductor matrix. This estimate strongly supports the idea of extrinsic centers related to Ge-pair, even if different hypothesis cannot be ruled out at the moment. Then in the following we will refer to them as Ge-centers emission.

Finally, we remark that this hyper-spectral imaging technique<sup>82</sup> allows the detection of complex dopant

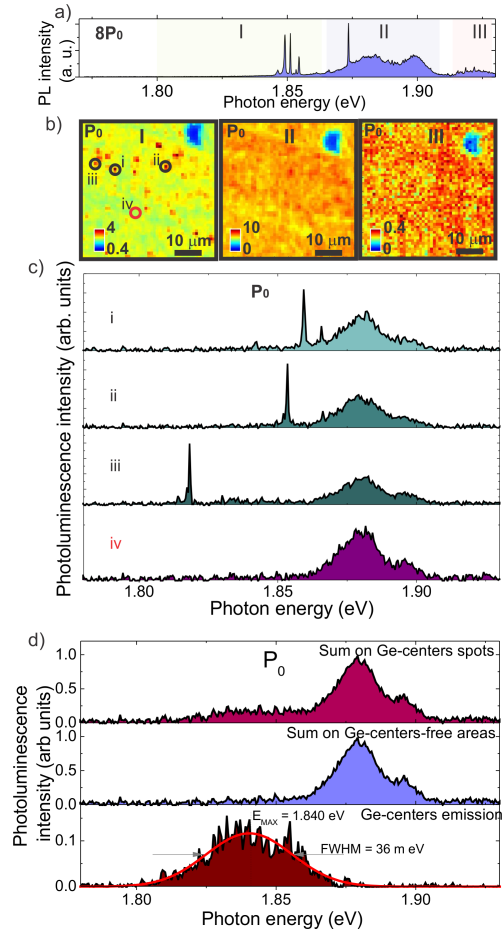


FIG. 3. a) Typical PL spectrum from the sample Ge 580 °C. The shaded areas I, II and III highlight the spectral intervals used to represent the spectral map shown in b). b)  $50 \times 50 \mu\text{m}^2$  spectral map integrated on the three different spectral intervals I, II and III highlighted in a). The excitation power density was  $P_0 = 5 \times 10^2 \text{ W/cm}^2$ . Similar maps but with a sharper spectral filtering are shown as an animated map in reference in the Supplementary Material 80 and 81. In the left panel I four spots (i, ii, iii, and iv) are highlighted and the corresponding extracted spectra are shown in c). d) Top panel: integrated and normalised emission from Ge-centers. Central panel: same as top panel but for Ge-centers-free areas (i.e. “bulk”  $\text{Al}_{0.3}\text{Ga}_{0.7}\text{As}$ ). Bottom panel: Isolated Ge-centers emission obtained as intensity difference between the two spectra in top and middle panels. The continuous red line is a Gaussian fit to the data.

impurities<sup>66</sup> with an extremely high sensitivity (note that the most accurate SIMS measurements can reach  $\sim 10^{13} \text{cm}^{-3}$ ). Differently from conventional near-field microscopy techniques for doping detection,<sup>46</sup> we can gather additional information about the energy of each defect within the energy band-gap of the host material and thus, *a posteriori*, we can re-build the full spectrum of the Ge-centers (see Fig. 3d)).

Combining the spectral information with the mapping over large areas of the sample, a precise characterization of the ensemble emission can be extracted despite the very low density of the Ge-centers. As a matter of fact standard macro-PL

measurements do not allow to extract the spectral emission band of these Ge centers.<sup>67</sup> The basic idea is to sum up only the micro-PL spectra arising from points containing the Ge-centers emission. This means that within the two  $50 \times 50 \mu\text{m}^2$  spectral maps, containing 2500 different points each, we operate a careful selection of 150 micro-PL spectra corresponding to individual Ge-centers emission. In this way we can build *a posteriori* a *pseudo-macro-PL* spectrum by summing them and normalising the total spectrum to its maximum intensity.

The result of this operation is shown in the top panel (*Sum on Ge-centers spots*) of Fig.3 d). The same procedure is applied to micro-PL spectra where no localised and sharp emission is present (*Sum on Ge-centers-free areas*), thus recovering the “bulk”-like emission of  $\text{Al}_{0.3}\text{Ga}_{0.7}\text{As}$ . This is shown in the central panels of Fig.3 d). Clearly the emission of the sharp lines is perfectly rejected in these spectra where only DA-Ge, DA-C and Bex are visible.

The large broadening of the PL band of the Ge-centers, may reflect either random distribution of the ion-to-ion distance  $d_{\text{Ge}-\text{Ge}}$  of the Ge-centers in the host material or the spectral diffusion associated with stochastic variations of the electric field<sup>83-92</sup> and/or alloy around the Ge-centers. The large broadening is also in stark contrast with what found in other systems like carbon<sup>62,63</sup> and copper<sup>64,65</sup> impurities in silicon or nitrogen-pairs in AlAs or GaAs,<sup>50,55,93</sup> featuring a well defined emission energy reflecting a limited number of optically active configurations for the impurities while it looks similar to what was found in Te-dyads in ZnSe,<sup>50,93,94</sup> Mn in ZnS,<sup>95</sup> and carbon-antisite pairs in SiC<sup>66</sup> where a relevant spread in the emission energy is present. At the same time, this large variation of excitonic recombination can be an advantage if a tuning or a selection of peculiar emission properties is needed. Note also that the emission of Ge-centers is related to the band gap of the host alloy, and then, in principle, a control of the emission energy could be obtained by tuning the Al content or preliminary using different III-V alloys. This is important for controlling the emission of these quantum sources to specific targets<sup>8,9</sup> or for coupling them to other optical devices (such as optical fibers or resonators).

#### IV. MULTI-EXCITON EMISSION

As found for other complex defects<sup>93,94</sup> the Ge-centers in study support charged excitons and multi-exciton features. We note that, considering a statistical analysis of  $\sim 150$  Ge-centers, practically all of them (more than 90%) show these features and we thus conclude that the Ge-centers in study support all the energy states typical of s-shell recombination: up to two bound electrons and two holes (respectively in conduction and valence band). A preliminary assignment of neutral exciton, biexciton and charged exciton was previously done by power dependence and fine structure splitting measurements.<sup>67,68</sup> Here we complete the full picture of the electronic states of the s-shell addressing both the positive ( $X^+$ ) and negative ( $X^-$ ) charged exciton levels. At the same time, we evaluate the capture volume and the carrier localization through the analysis of the saturation power.<sup>96</sup>

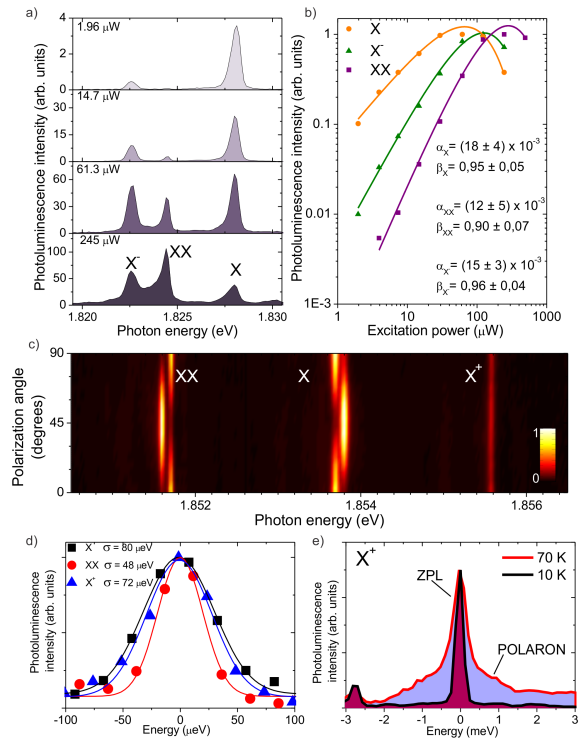


FIG. 4. a) Series of PL spectra at different excitation power of an individual Ge-impurity exhibiting  $X^-$ ,  $XX$  and  $X$  recombination. b) Summary of the PL intensity as a function of the excitation power  $\mathcal{P}$  of the data reported in a). Symbols are the experimental data while the lines represent Poissonian fit. c) Polarization map of an individual Ge-impurity exhibiting  $XX$ ,  $X$  and  $X^+$  recombination. d)  $X$ ,  $XX$  and  $X^+$  normalized and energy- shifted emission at 10 K. The continuous lines are Gaussian fit to the data. e) Normalised spectra of  $X^+$  emission at 10 K and 70 K. The zero-phonon-line (ZPL) and the polaron emission are highlighted.

In Fig.4 a) we show typical PL spectra of an individual Ge-center at different power density. The emission clearly shows additional spectral components ascribed to biexcitons and charged exciton complexes.<sup>68</sup> The corresponding evolution of the PL intensities with power is displayed in Fig.4 b). Here, according to a Poissonian model for the level occupation probability<sup>96</sup> the three main PL lines follow slightly different filling dynamics (the fits shown in Fig.4 b) correspond to  $I_{PL} \propto (\alpha \mathcal{P}^\beta)^m \exp(-(\alpha \mathcal{P}^\beta)^m)$  where  $m = 1, 1.5, 2$  corresponds respectively to one exciton ( $X$ ), one exciton plus a spectator charge ( $X^\pm$ ) and two excitons ( $XX$ );  $\mathcal{P}$  is the excitation power;  $\alpha$  and  $\beta$  are fitting parameters describing the capture mechanism and their corresponding values extracted from the fit are directly reported on Fig.4 b)). The dependence on the excitation power,<sup>96</sup> the line broadening,<sup>86</sup> and the relative spectral position<sup>97</sup> leads us to the attribution of the lines to  $X^-$ ,  $XX$ , and  $X$ . The  $X$  line reported in Fig. 4 b) shows a saturation power of about  $\mathcal{P}_{sat} \simeq 0.6$  mW while slightly different values (not shown) were observed for other Ge-centers (from  $\sim 0.05$  up to  $\sim 1$  mW). This feature possibly reflects a different capture efficiency due to the presence of extrinsic ef-

fects related to disorder in the electrostatic environment of the emitters.<sup>88,90–92,96,98</sup>

The saturation power of X (i.e. the value  $\mathcal{P}_{sat}$  for the maximum occupation probability) allows to estimate the capture length of the Ge-centers.<sup>96</sup> From the typical values of  $\mathcal{P}_{sat}$  for X and taking into account the experimental conditions, we estimate a capture length ranging from  $\sim 30$  nm up to  $\sim 10$  nm, similar or smaller of that found for GaAs/Al<sub>0.3</sub>Ga<sub>0.7</sub>As epitaxial quantum dots<sup>96,99,100</sup> investigated with the same experimental apparatus and with similar excitation conditions.

Clearcut attribution of the exciton-biexciton cascade and charged exciton comes from fine structure splitting measurements: an example of a different individual Ge-center showing X<sup>+</sup>, XX, and X is reported in Fig. 4 c). The X and XX lines shifts symmetrically when changing the detected polarization angle, while the X<sup>+</sup> does not shift.<sup>37,43,86,96</sup>

Let us now consider the line broadening of the different recombination lines as an additional key for attributing the excitonic complexes (see Fig. 4 d). From a statistical point of view we observe a wide spread of values of the linewidth ranging from few tens up to few hundreds of  $\mu\text{eV}$ , still the order from the sharper to the broader lines among the different excitonic complexes does not vary:  $\sigma_{X^-} \sim \sigma_X > \sigma_{X^+} > \sigma_{XX}$  (for the sake of thoroughness we note that X<sup>-</sup> featuring larger or smaller broadening with respect to the corresponding X can be found). The gaussian broadening of the low temperature PL emission of individual excitonic transitions is commonly ascribed to spectral diffusion and<sup>83–92</sup> a hierarchical broadening (showing  $\sigma_{X^-} \sim \sigma_X > \sigma_{X^+} \sim \sigma_{XX}$ ) has been already found in epitaxial quantum dots<sup>86,87,101,102</sup> and impurities.<sup>72</sup> This behaviour can be explained in terms of a *selective* quantum confined Stark effect induced by the presence of charged defects in the semiconductor matrix.<sup>86,87</sup> The relative position of the charged trap results in a different Stark shift amplitude (and eventually sign) for each excitonic complex. On one side, the analogy with QDs is expected for any strongly confining potential able to localize the electrons and holes at the nm scale, as in the case of the Ge-centers in study. On the other side, we did use this analogy with QDs in order to attribute the emission lines to different excitonic complexes. In this respect the hierarchical broadening is a confirmation of the soundness of our attribution.

In view of possible integration in optoelectronic devices it is also needed to increase the operation temperature of the quantum sources as much as possible. Indeed we were able to follow the emission of the Ge-centers up to 70 K. Following the temperature-induced red-shift of any excitonic recombination we observe an initial linear decrease in energy and then a steeper quadratic decrease (as reasonably expected for electronic transitions in semiconducting materials according to the Varshni empirical law of AlGaAs alloy).<sup>103,104</sup> While at low temperature only a sharp line is visible, with a spectral broadening limited by our low resolution (in these data) at higher temperature we assist to a slight broadening of the central sharp line together with the onset of a broad pedestal.<sup>84,105–109</sup> These features can be interpreted in terms of electron-acoustic phonon interaction: in analogy with epitaxial quantum dots, we assign the sharp component of the single Ge-impurities

emission to the exciton zero phonon line (ZPL in Fig. 4e) while the sidebands to a superposition of acoustic phonon replicas. The still sharp emission at T = 70 K and the limited thermal quenching of the PL (quite similar to what observed in GaAs QDs) lead us to state the possibility to use the Ge-centers as quantum emitters at liquid nitrogen temperature.

## V. BINDING ENERGY OF XX, X<sup>+</sup> AND X<sup>-</sup>

We now address the issue of the Coulombic interactions between electrons and holes trapped by Ge-impurities which are responsible for the lifted degeneracy of the neutral exciton state as well as for the energy re-normalization of the electronic states within individual impurity centers.

Due to asymmetries in the confinement potential and local strain accumulation the two spin states of the bright neutral exciton are split by the so called fine structure splitting (FSS) associated to the exchange interaction;<sup>26,35–37,43,55,110</sup> for the Ge-centers in study, it has been shown that the FSS is in the  $\sim 100$   $\mu\text{eV}$  range (see Fig. 4 c)).<sup>68</sup>

The so called exciton binding energy is simply defined as the energy shift with respect to the corresponding neutral exciton line ( $BE_{XX} = E_X - E_{XX}$ ). Similarly, one can define the charged exciton binding energy as  $BE_{X^\pm} = E_X - E_{X^\pm}$ . The binding energy arises from the complicate interplay of direct Coulombic interactions, exchange and correlation typical of each excitonic species.<sup>37,42,44,93,97,111–115</sup>

Generally speaking three scenarios can occur, the binding energy is positive, zero or negative. In the case of the biexciton complex these cases are represented in Fig. 5 a) also including the presence of FSS (not in scale). In the left panel of Fig. 5 a) is displayed the situation of a XX having positive binding energy  $BE_{XX} > 0$ . In this condition (if FSS  $\neq 0$ ) the emitted photons in the biexciton cascade are discernible in energy and polarization. If instead the FSS vanishes, the XX and X photons are polarization-entangled.<sup>4,15,20,25–28,34,38</sup> In the central panel of Fig. 5 a) is shown a XX with a zero binding energy  $BE_{XX} = 0$  where the emission energy of H-(V)polarised XX photons matches that of the V-(H) polarised X photon. The two photons are not distinguishable in energy and thus polarization entanglement can be recovered with a time-reordering scheme.<sup>39,40</sup> Finally, in the right panel, it is shown the case of negative binding energy ( $BE_{XX} < 0$ ); here the same considerations made for the left panel apply. Therefore, in view of realising a quantum source of entangled photons pairs, the condition can be  $FSS = 0$  or  $BE_{XX} = 0$ .

Let us now consider the experimental data for the binding energies of excitonic complex localised at the Ge-centers. As most of these transitions were mainly attributed on the base of the power dependence it is usually easy to have a clear attribution of X and XX while the X<sup>+</sup> and X<sup>-</sup> attributions are sometimes less certain. Disregarding the ambiguous cases leads to a lower statistic for X<sup>+</sup> and X<sup>-</sup>. Summary of the data with excitonic recombination ranging from  $\sim 1.81$  eV to  $\sim 1.86$  eV is given in Fig. 5 a). Pronounced features emerging from this analysis are summarized as follows:  
-the binding energy of X<sup>+</sup> shows a decreasing trend when in-

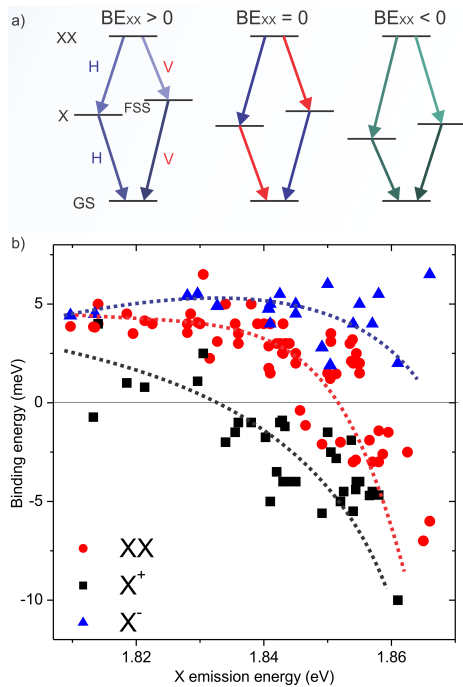


FIG. 5. a) Scheme of X and XX energy levels for three different binding energy of XX; from left to right: positive, zero, and negative. V and H highlight the linear polarization of the emitted photons. b) Binding energy of X<sup>-</sup>, X<sup>+</sup> and XX. Dotted lines are guides to the eyes.

creasing X emission energy, from  $\sim +1$  meV to  $\sim -5$  meV, with a transition from binding to anti-binding.

-The XX state shows a binding energy of about  $\sim +4$  meV at low energy and abruptly evolves toward negative values above 1.855 eV reaching the negative value of about  $\sim -6$  meV with a steep trend.

-The binding energy of X<sup>-</sup> is always positive, thus X<sup>-</sup> forms a bound state. Its evolution with the 3D confinement is quite constant even if the number of points is quite small due to the problematic attribution of this line.

Comparing these results with calculations and experimental data for quantum dots or monolayer fluctuation of quantum wells<sup>97,112–116</sup> we can see a remarkable agreement with the behaviour predicted and measured for a truly 3D confinement<sup>97,112</sup> (i.e. a small quantum dot without a wetting layer). XX and X<sup>+</sup> show a steep reduction in the binding energy and eventually a change of its sign. This is interpreted as a consequence of the dominant exciton mean-field interaction present in a spherical confining well, reflecting a strong carrier localization in all the spatial directions. Nevertheless, as a consequence of the larger effective mass of holes with respect to electrons, the same mean field would serve as a repulsive force for a hole and an attractive one for electrons thus leading to an opposite trend and sign for X<sup>+</sup> and X<sup>-</sup> binding energies.

These findings are in contrast with common epitaxial quantum dots with a weaker lateral confinement originated by a 2D wetting layer: in these cases a linear dependence of the

XX and X<sup>+</sup> binding energy as a function of the X emission is usually found together with a dominantly binding-nature of the XX state.<sup>42,44,97,115,116</sup>

We conclude that a strong carrier localization is present for high energy Ge-centers, while the positive values of the binding energy found at lower X emission energy suggests a recovered dominant effect of the correlation term. Most importantly, a XX state emitting at energies close to that of the corresponding X state can be achieved, thus allowing for an easier implementation of a *time reordering* scheme for entangled photons<sup>39,40</sup> eventually with the help of a (small) external field for the fine tuning.<sup>25,28,34</sup>

## VI. CONCLUSIONS

In conclusion we have shown that the single photon emitters recently reported<sup>67,68</sup> are related to Ge-centers and come from unintentional contamination of the III-V layers grown on germanium substrates. These centers provide a valuable alternative to epitaxial quantum dots for the implementation of different carrier states such as X, XX, X<sup>+</sup> and X<sup>-</sup> and, in analogy with similar impurities, could be in principle implemented through ionic implantation.<sup>60,62–66</sup> Due to the strong carrier confinement the Ge-centers feature similar properties to the epitaxial quantum dot counterpart, present a line broadening dominated by a quantum-confined Stark effect at low temperature and a phonon-coupling at higher temperatures. The optical properties of the excitonic recombination from Ge-centers are quite good: linewidth as sharp as 40  $\mu$ eV can be found at high excitation power densities and low temperature, the emission is still bright at 70 K, confirming the good thermal stability of this class of emitters. The electronic states populating the s-shell well agree with what found for a fully 3D confining potential in quantum dots and thus enable the implementation of quasi degenerate X and XX states.

Our findings suggest the use of the PL emission of Ge extrinsic centers in Al<sub>0.3</sub>Ga<sub>0.7</sub>As as a versatile platform for obtaining single photons on a large spectral range and entangled photons based on the *time reordering scheme*,<sup>39,40</sup> for spin-photon turn-stile devices and for slow-light when coupled with atomic vapours.<sup>8,9</sup> We stress that, differently from most III-V compounds where Stranski-Krastanov quantum dots are obtained, the emission of these Ge-centers well matches the highest detection efficiency of Si-based single photon detectors ensuring a high fidelity in the detection and not only in the preparation of the quantum state of the system.<sup>14</sup> Last but not least, these results have been obtained on silicon and germanium substrates opening up new avenues for the exploitation of quantum emitters within a device-friendly platform.

## ACKNOWLEDGMENTS

This work has been carried out thanks to the support of the European project *LASERLAB-EUROPE* (grant agreement no. 284464, EC's Seventh Framework).

- \* Corresponding author: Marco Abbarchi (marco.abbarchi@im2np.fr)
- † Corresponding author: Massimo Gurioli (gurioli@fi.infn.it)
- <sup>1</sup> A. Imamog, D. D. Awschalom, G. Burkard, D. P. DiVincenzo, D. Loss, M. Sherwin, A. Small, *et al.*, *Physical Review Letters* **83**, 4204 (1999).
  - <sup>2</sup> C. H. Bennett, *Physics Today* **48**, 24 (2008).
  - <sup>3</sup> M. A. Nielsen and I. L. Chuang, *Quantum computation and quantum information* (Cambridge university press, 2010).
  - <sup>4</sup> X. Li, Y. Wu, D. Steel, D. Gammon, T. Stievater, D. Katzer, D. Park, C. Piermarocchi, and L. Sham, *Science* **301**, 809 (2003).
  - <sup>5</sup> D. Fattal, E. Diamanti, K. Inoue, and Y. Yamamoto, *Physical review letters* **92**, 037904 (2004).
  - <sup>6</sup> A. Politi, J. C. Matthews, and J. L. O'Brien, *Science* **325**, 1221 (2009).
  - <sup>7</sup> F. Troiani, U. Hohenester, and E. Molinari, *Physical Review B* **62**, R2263 (2000).
  - <sup>8</sup> N. Akopian, L. Wang, A. Rastelli, O. Schmidt, and V. Zwiller, *Nature Photonics* **5**, 230 (2011).
  - <sup>9</sup> P. Siyushev, G. Stein, J. Wrachtrup, and I. Gerhardt, *Nature* **509**, 66 (2014).
  - <sup>10</sup> K. De Greve, L. Yu, P. L. McMahon, J. S. Pelc, C. M. Natarajan, N. Y. Kim, E. Abe, S. Maier, C. Schneider, M. Kamp, *et al.*, *Nature* **491**, 421 (2012).
  - <sup>11</sup> W. Gao, P. Fallahi, E. Togan, J. Miguel-Sanchez, and A. Imamoglu, *Nature* **491**, 426 (2012).
  - <sup>12</sup> R. J. Warburton, *Nature materials* **12**, 483 (2013).
  - <sup>13</sup> B. Lounis and M. Orrit, *Reports on Progress in Physics* **68**, 1129 (2005).
  - <sup>14</sup> M. Eisaman, J. Fan, A. Migdall, and S. Polyakov, *Review of Scientific Instruments* **82**, 071101 (2011).
  - <sup>15</sup> G. Chen, N. Bonadeo, D. Steel, D. Gammon, D. Katzer, D. Park, and L. Sham, *Science* **289**, 1906 (2000).
  - <sup>16</sup> V. Zwiller, H. Blom, P. Jonsson, N. Panev, S. Jeppesen, T. Tsegaye, E. Goobar, M.-E. Pistol, L. Samuelson, and G. Björk, *Applied Physics Letters* **78**, 2476 (2001).
  - <sup>17</sup> D. Regelman, U. Mizrahi, D. Gershoni, E. Ehrenfreund, W. Schoenfeld, and P. Petroff, *Physical review letters* **87**, 257401 (2001).
  - <sup>18</sup> T. Stievater, X. Li, D. G. Steel, D. Gammon, D. Katzer, D. Park, C. Piermarocchi, and L. Sham, *Physical Review Letters* **87**, 133603 (2001).
  - <sup>19</sup> X. Brokmann, G. Messin, P. Desbiolles, E. Giacobino, M. Dahan, and J. Hermier, *New Journal of Physics* **6**, 99 (2004).
  - <sup>20</sup> R. M. Stevenson, R. J. Young, P. Atkinson, K. Cooper, D. A. Ritchie, and A. J. Shields, *Nature* **439**, 179 (2006).
  - <sup>21</sup> H. Kumano, S. Kimura, M. Endo, H. Sasakura, S. Adachi, S. Muto, and I. Suemune, *Journal of Nanoelectronics and Optoelectronics* **1**, 39 (2006).
  - <sup>22</sup> M. Abbarchi, C. Mastrandrea, A. Vinattieri, S. Sanguinetti, T. Mano, T. Kuroda, N. Koguchi, K. Sakoda, and M. Gurioli, *Physical Review B* **79**, 085308 (2009).
  - <sup>23</sup> T. Kuroda, T. Belhadj, M. Abbarchi, C. Mastrandrea, M. Gurioli, T. Mano, N. Ikeda, Y. Sugimoto, K. Asakawa, N. Koguchi, *et al.*, *Physical Review B* **79**, 035330 (2009).
  - <sup>24</sup> A. Ulhaq, S. Weiler, S. Ulrich, R. Roßbach, M. Jetter, and P. Michler, *Nature Photonics* **6**, 238 (2012).
  - <sup>25</sup> R. Trotta, P. Atkinson, J. Plumhof, E. Zallo, R. Rezaev, S. Kumar, S. Baunack, J. Schroeter, A. Rastelli, and O. Schmidt, *Advanced Materials* **24**, 2668 (2012).
  - <sup>26</sup> T. Kuroda, T. Mano, N. Ha, H. Nakajima, H. Kumano, B. Urbaszek, M. Jo, M. Abbarchi, Y. Sakuma, K. Sakoda, *et al.*, *Physical Review B* **88**, 041306 (2013).
  - <sup>27</sup> H. Jayakumar, A. Predojević, T. Huber, T. Kauten, G. S. Solomon, and G. Weihs, *Phys. Rev. Lett.* **110**, 135505 (2013).
  - <sup>28</sup> R. Trotta, J. S. Wildmann, E. Zallo, O. G. Schmidt, and A. Rastelli, *Nano letters* (2014).
  - <sup>29</sup> S. Birindelli, M. Felici, J. S. Wildmann, A. Polimeni, M. Capizzi, A. Gerardino, S. Rubini, F. Martelli, A. Rastelli, and R. Trotta, *Nano Letters* **14**, 1275 (2014), <http://pubs.acs.org/doi/pdf/10.1021/nl404196y>.
  - <sup>30</sup> A. Högele, C. Galland, M. Winger, and A. Imamoglu, *Physical review letters* **100**, 217401 (2008).
  - <sup>31</sup> T. Basché, W. Moerner, M. Orrit, and H. Talon, *Physical review letters* **69**, 1516 (1992).
  - <sup>32</sup> C. Brunel, B. Lounis, P. Tamarat, and M. Orrit, *Physical Review Letters* **83**, 2722 (1999).
  - <sup>33</sup> B. Lounis and W. Moerner, *Nature* **407**, 491 (2000).
  - <sup>34</sup> R. Trotta, E. Zallo, C. Ortix, P. Atkinson, J. Plumhof, J. Van den Brink, A. Rastelli, and O. Schmidt, *Physical review letters* **109**, 147401 (2012).
  - <sup>35</sup> T. Mano, M. Abbarchi, T. Kuroda, B. McSkimming, A. Ohtake, K. Mitsuishi, and K. Sakoda, *Applied physics express* **3**, 065203 (2010).
  - <sup>36</sup> N. Ha, X. Liu, T. Mano, T. Kuroda, K. Mitsuishi, A. Castellano, S. Sanguinetti, T. Noda, Y. Sakuma, and K. Sakoda, *Applied Physics Letters* **104**, 143106 (2014).
  - <sup>37</sup> X. Liu, N. Ha, H. Nakajima, T. Mano, T. Kuroda, B. Urbaszek, H. Kumano, I. Suemune, Y. Sakuma, and K. Sakoda, *Physical Review B* **90**, 081301 (2014).
  - <sup>38</sup> N. Akopian, N. Lindner, E. Poem, Y. Berlatzky, J. Avron, D. Gershoni, B. Gerardot, and P. Petroff, *Physical review letters* **96**, 130501 (2006).
  - <sup>39</sup> F. Troiani and C. Tejedor, *Physical Review B* **78**, 155305 (2008).
  - <sup>40</sup> J. E. Avron, G. Bisker, D. Gershoni, N. H. Lindner, E. A. Meirom, and R. J. Warburton, *Physical review letters* **100**, 120501 (2008).
  - <sup>41</sup> S. Rodt, R. Heitz, A. Schliwa, R. Sellin, F. Guffarth, and D. Bimberg, *Physical Review B* **68**, 035331 (2003).
  - <sup>42</sup> S. Rodt, A. Schliwa, K. Pötschke, F. Guffarth, and D. Bimberg, *Physical Review B* **71**, 155325 (2005).
  - <sup>43</sup> S. Rodt, R. Seguin, A. Schliwa, F. Guffarth, K. Pötschke, U. Pohl, and D. Bimberg, *Journal of luminescence* **122**, 735 (2007).
  - <sup>44</sup> A. Schliwa, M. Winkelkemper, and D. Bimberg, *Physical Review B* **79**, 075443 (2009).
  - <sup>45</sup> D. Thomas and J. Hopfield, *Physical Review* **150**, 680 (1966).
  - <sup>46</sup> M. R. Castell, D. A. Muller, and P. M. Voyles, *Nature materials* **2**, 129 (2003).
  - <sup>47</sup> C. F. Klingshirn, *Semiconductor optics*, Vol. 3 (Springer, 2007).
  - <sup>48</sup> P. M. Koenraad and M. E. Flatté, *Nature materials* **10**, 91 (2011).
  - <sup>49</sup> K. Sanaka, A. Pawlis, T. D. Ladd, K. Lischka, and Y. Yamamoto, *Phys. Rev. Lett.* **103**, 053601 (2009).
  - <sup>50</sup> A. Muller, P. Bianucci, C. Piermarocchi, M. Fornari, I. Robin, R. André, and C. Shih, *Physical Review B* **73**, 081306 (2006).
  - <sup>51</sup> S. Francoeur, J. Klem, and A. Mascarenhas, *Physical review letters* **93**, 067403 (2004).
  - <sup>52</sup> M. Ikezawa, Y. Sakuma, L. Zhang, Y. Sone, T. Mori, T. Hamano, M. Watanabe, K. Sakoda, and Y. Masumoto, *Applied physics letters* **100**, 042106 (2012).
  - <sup>53</sup> L. Zhang, M. Ikezawa, T. Mori, S. Umehara, Y. Sakuma, K. Sakoda, and Y. Masumoto, *Japanese Journal of Applied Physics* **52**, 04CG11 (2013).



- <sup>54</sup> G. Éthier-Majcher, P. St-Jean, G. Boso, A. Tosi, J. Klem, and S. Francoeur, *Nature communications* **5** (2014).
- <sup>55</sup> M. Jo, T. Mano, T. Kuroda, Y. Sakuma, and K. Sakoda, *Applied Physics Letters* **102**, 062107 (2013).
- <sup>56</sup> C. Kurtsiefer, S. Mayer, P. Zarda, and H. Weinfurter, *Physical Review Letters* **85**, 290 (2000).
- <sup>57</sup> A. Beveratos, S. Kühn, R. Brouri, T. Gacoin, J.-P. Poizat, and P. Grangier, *The European Physical Journal D-Atomic, Molecular, Optical and Plasma Physics* **18**, 191 (2002).
- <sup>58</sup> V. Jacques, E. Wu, F. Grosshans, F. Treussart, P. Grangier, A. Aspect, and J.-F. Roch, *Science* **315**, 966 (2007).
- <sup>59</sup> S. Castelletto, I. Aharonovich, B. Gibson, B. Johnson, and S. Praver, *Physical review letters* **105**, 217403 (2010).
- <sup>60</sup> M. Lesik, P. Spinicelli, S. Pezzagna, P. Happel, V. Jacques, O. Sallord, B. Rasser, A. Delobbe, P. Sudraud, A. Tallaire, *et al.*, *physica status solidi (a)* **210**, 2055 (2013).
- <sup>61</sup> P. Spinicelli, A. Dréau, L. Rondin, F. Silva, J. Achard, S. Xavier, S. Bansropun, T. Debuisschert, S. Pezzagna, J. Meijer, *et al.*, *New Journal of Physics* **13**, 025014 (2011).
- <sup>62</sup> S. G. Cloutier, P. A. Kosyrev, and J. Xu, *Nature materials* **4**, 887 (2005).
- <sup>63</sup> D. D. Berhanuddin, M. A. Lourenço, R. M. Gwilliam, and K. P. Homewood, *Advanced Functional Materials* **22**, 2709 (2012).
- <sup>64</sup> J. Weber, H. Bauch, and R. Sauer, *Physical Review B* **25**, 7688 (1982).
- <sup>65</sup> H. Sumikura, E. Kuramochi, H. Taniyama, and M. Notomi, *Scientific reports* **4** (2014).
- <sup>66</sup> S. Castelletto, B. Johnson, V. Ivády, N. Stavrias, T. Umeda, A. Gali, and T. Ohshima, *Nature materials* **13**, 151 (2014).
- <sup>67</sup> S. Minari, L. Cavigli, F. Sarti, M. Abbarchi, N. Accanto, G. M. Matutano, S. Bietti, S. Sanguinetti, A. Vinattieri, and M. Gurioli, *Applied physics letters* **101**, 172105 (2012).
- <sup>68</sup> F. Sarti, G. M. Matutano, D. Bauer, N. Dotti, S. Bietti, G. Isella, A. Vinattieri, S. Sanguinetti, and M. Gurioli, *Journal of Applied Physics* **114**, 224314 (2013).
- <sup>69</sup> N. Chand, J. Klem, T. Henderson, and H. Morkoc, *Journal of applied physics* **59**, 3601 (1986).
- <sup>70</sup> R. Sieg, S. Ringel, S. Ting, E. Fitzgerald, and R. Sacks, *Journal of electronic materials* **27**, 900 (1998).
- <sup>71</sup> M. Heiss, Y. Fontana, A. Gustafsson, G. Wüst, C. Magen, D. O'Regan, J. Luo, B. Ketterer, S. Conesa-Boj, A. Kuhlmann, *et al.*, *Nature materials* **12**, 439 (2013).
- <sup>72</sup> P. Corfdir, Y. Fontana, B. Van Hattem, E. Russo-Averchi, M. Heiss, A. F. i Morral, and R. Phillips, *Applied Physics Letters* **105**, 223111 (2014).
- <sup>73</sup> M. Veta, K. Kanzaki, Y. Toyozawa, and E. Hanamura, *Electromagnetic* , 305 (1985).
- <sup>74</sup> L. Pavesi and M. Guzzi, *Journal of Applied Physics* **75**, 4779 (1994).
- <sup>75</sup> K. Ploog, A. Fischer, and H. Künzel, *Journal of The Electrochemical Society* **128**, 400 (1981).
- <sup>76</sup> G. Oelgart, B. Lippold, R. Heilmann, H. Neumann, and B. Jacobs, *physica status solidi (a)* **115**, 257 (1989).
- <sup>77</sup> P. Mooney, *Journal of Applied Physics* **67**, R1 (1990).
- <sup>78</sup> S. T. Pantelides, *Deep centers in semiconductors* (CRC Press, 1992).
- <sup>79</sup> H. Feichtinger, *Deep Centers in Semiconductors* (Wiley Online Library).
- <sup>80</sup> [https://dl.dropboxusercontent.com/u/7275038/Map1\\_HQ.gif](https://dl.dropboxusercontent.com/u/7275038/Map1_HQ.gif), .
- <sup>81</sup> [https://dl.dropboxusercontent.com/u/7275038/Map2\\_HQ.gif](https://dl.dropboxusercontent.com/u/7275038/Map2_HQ.gif), .
- <sup>82</sup> W. Bao, M. Melli, N. Caselli, F. Riboli, D. Wiersma, M. Stafaroni, H. Choo, D. Ogletree, S. Aloni, J. Bokor, *et al.*, *Science* **338**, 1317 (2012).
- <sup>83</sup> R. Neuhauser, K. Shimizu, W. Woo, S. Empedocles, and M. Bawendi, *Physical review letters* **85**, 3301 (2000).
- <sup>84</sup> A. Berthelot, I. Favero, G. Cassaboïs, C. Voisin, C. Delalande, P. Roussignol, R. Ferreira, and J.-M. Gérard, *Nature Physics* **2**, 759 (2006).
- <sup>85</sup> L. Coolen, X. Brokmann, and J.-P. Hermier, *Physical Review A* **76**, 033824 (2007).
- <sup>86</sup> M. Abbarchi, F. Troiani, C. Mastrandrea, G. Goldoni, T. Kuroda, T. Mano, K. Sakoda, N. Koguchi, S. Sanguinetti, A. Vinattieri, *et al.*, *Applied physics letters* **93**, 162101 (2008).
- <sup>87</sup> T. Mano, M. Abbarchi, T. Kuroda, C. Mastrandrea, A. Vinattieri, S. Sanguinetti, K. Sakoda, and M. Gurioli, *Nanotechnology* **20**, 395601 (2009).
- <sup>88</sup> G. Sallen, A. Tribu, T. Aichele, R. André, L. Besombes, C. Bougerol, M. Richard, S. Tatarenko, K. Kheng, and J.-P. Poizat, *Nature Photonics* **4**, 696 (2010).
- <sup>89</sup> M. Abbarchi, T. Kuroda, R. Duval, T. Mano, and K. Sakoda, *Review of Scientific Instruments* **82**, 073103 (2011).
- <sup>90</sup> H.-S. Nguyen, G. Sallen, C. Voisin, P. Roussignol, C. Diederichs, and G. Cassaboïs, *Physical review letters* **108**, 057401 (2012).
- <sup>91</sup> H. S. Nguyen, G. Sallen, M. Abbarchi, R. Ferreira, C. Voisin, P. Roussignol, G. Cassaboïs, and C. Diederichs, *Physical Review B* **87**, 115305 (2013).
- <sup>92</sup> C. Matthiesen, M. J. Stanley, M. Hugues, E. Clarke, and M. Atature, *Scientific reports* **4** (2014).
- <sup>93</sup> S. Marcet, R. André, and S. Francoeur, *Physical Review B* **82**, 235309 (2010).
- <sup>94</sup> S. Marcet, C. Ouellet-Plamondon, G. Éthier-Majcher, P. Saint-Jean, R. André, J. Klem, and S. Francoeur, *Physical Review B* **82**, 235311 (2010).
- <sup>95</sup> S. Sapa, A. Prakash, A. Ghangrekar, N. Periasamy, and D. Sarma, *The Journal of Physical Chemistry B* **109**, 1663 (2005).
- <sup>96</sup> M. Abbarchi, C. Mastrandrea, T. Kuroda, T. Mano, A. Vinattieri, K. Sakoda, and M. Gurioli, *Journal of Applied Physics* **106**, 053504 (2009).
- <sup>97</sup> M. Abbarchi, T. Kuroda, T. Mano, K. Sakoda, C. A. Mastrandrea, A. Vinattieri, M. Gurioli, and T. Tsuchiya, *Physical Review B* **82**, 201301 (2010).
- <sup>98</sup> M. Abbarchi, T. Kuroda, T. Mano, M. Gurioli, and K. Sakoda, *Physical Review B* **86**, 115330 (2012).
- <sup>99</sup> L. Cavigli, S. Bietti, N. Accanto, S. Minari, M. Abbarchi, G. Isella, C. Frigeri, A. Vinattieri, M. Gurioli, and S. Sanguinetti, *Applied physics letters* **100**, 231112 (2012).
- <sup>100</sup> N. Accanto, S. Minari, L. Cavigli, S. Bietti, G. Isella, A. Vinattieri, S. Sanguinetti, and M. Gurioli, *Applied Physics Letters* **102**, 053109 (2013).
- <sup>101</sup> S. Adachi, N. Yatsu, R. Kaji, S. Muto, and H. Sasakura, *Applied Physics Letters* **91**, 161910 (2007).
- <sup>102</sup> H. Kumano, H. Kobayashi, S. Ekuni, Y. Hayashi, M. Jo, H. Sasakura, S. Adachi, S. Muto, and I. Suemune, *Physical Review B* **78**, 081306 (2008).
- <sup>103</sup> Y. Varshni, *Physica* **34**, 149 (1967).
- <sup>104</sup> S. Sanguinetti, E. Poliani, M. Bonfanti, M. Guzzi, E. Grilli, M. Gurioli, and N. Koguchi, *Physical review B* **73**, 125342 (2006).
- <sup>105</sup> T. Takagahara, *Phys. Rev. B* **60**, 2638 (1999).
- <sup>106</sup> B. Krummheuer, V. M. Axt, and T. Kuhn, *Physical Review B* **65**, 195313 (2002).
- <sup>107</sup> I. Favero, G. Cassaboïs, R. Ferreira, D. Darson, C. Voisin, J. Tignon, C. Delalande, G. Bastard, P. Roussignol, and J. Gérard, *Physical Review B* **68**, 233301 (2003).
- <sup>108</sup> E. Muljarov and R. Zimmermann, *Physical review letters* **93**,

- 237401 (2004).
- <sup>109</sup> M. Abbarchi, M. Gurioli, A. Vinattieri, S. Sanguinetti, M. Bonfanti, T. Mano, K. Watanabe, T. Kuroda, and N. Koguchi, *Journal of applied physics* **104**, 023504 (2008).
- <sup>110</sup> M. Abbarchi, C. Mastrandrea, T. Kuroda, T. Mano, K. Sakoda, N. Koguchi, S. Sanguinetti, A. Vinattieri, and M. Gurioli, *Physical Review B* **78**, 125321 (2008).
- <sup>111</sup> A. Franceschetti, H. Fu, L. Wang, and A. Zunger, *Physical Review B* **60**, 1819 (1999).
- <sup>112</sup> T. Tsuchiya, *Physica E: Low-dimensional Systems and Nanostructures* **7**, 470 (2000).
- <sup>113</sup> D. Regelman, E. Dekel, D. Gershoni, E. Ehrenfreund, A. Williamson, J. Shumway, A. Zunger, W. Schoenfeld, and P. Petroff, *Physical Review B* **64**, 165301 (2001).
- <sup>114</sup> A. Filinov, C. Riva, F. Peeters, Y. E. Lozovik, and M. Bonitz, *Physical Review B* **70**, 035323 (2004).
- <sup>115</sup> G. Moody, R. Singh, H. Li, I. Akimov, M. Bayer, D. Reuter, A. Wieck, A. Bracker, D. Gammon, and S. Cundiff, *Physical Review B* **87**, 041304 (2013).
- <sup>116</sup> M. Abbarchi, T. Kuroda, T. Mano, K. Sakoda, and M. Gurioli, *Physical Review B* **81**, 035334 (2010).